A ES
ISSN: 2096-3246
Volume 54, Issue 02, December, 2022
Special Issue

PHOTON-ATOM INTERACTION AND SUBSEQUENT PROCESSES IN X-RAY ENERGY REGION- THEORETICAL ASPECT

Gurjot Singh
SGT University, Gurugram, India

U.S. Yadav
Babu Banarasi Das University, Lucknow (U.P.), India

*Corresponding email ID: gurjot.phy@gmail.com

Abstract

This chapter covers the theoretical approach of photon-atom interaction and subsequent inner shell vacancy decay processes. The foremost interaction processes, *viz.*, photoionisation and scattering processes have been discussed. The near edge processes, *viz.*, resonant Raman scattering (RRS) is also explained. These processes become significant at the incident photon energies in the vicinity of the ionization threshold of the target atom. The X-ray diffraction process is explained. The powder XRD gives information about the crystal lattice dimensions, which is further used to identify the chemical phase of the element present in the sample.

Keywords: Photon-atom interaction, Rayleigh scattering, Compton Scattering, Resonant raman scattering, Inner shell vacancy phenomena.

1. Introduction

Since discovery of X-rays in Nov. 1895, interaction of X-ray photons with the matter has been widely studied. The X-rays are basically electromagnetic radiations (range of energies ~1-100 keV) which interact mainly with the electrons in atoms constituting the material. The interaction of X-rays with matter represents one of the most varied classes of phenomena in Physics.

The interaction can primarily be a scattering event, in which a part of energy is imparted any of the electrons associated with it; or it may be essentially an absorption process, in which the energy of the photon will be transferred to one of its electrons. When interaction of the X-ray photons involves material in the form of a periodic array atoms bound by chemical bonds or other interatomic forces (crystal lattice), the planes in the periodic structure scatters the incident X-rays. The parallel scattered X-rays result in the interference pattern and the process is called Bragg's diffraction. The phenomena was discovered in 1912 and provided a new method for investigating the fine lattice structure of material. The crystal lattice has planes in various orientations, which result in giving a variety of intensity patterns providing information about the structure of lattice. The absorption and scattering processes in crystals forms the basis of X-ray Crystallography. Interaction of photons with individual atoms and periodic array of a large number of atoms play role in development of various analytical

and diagnostic techniques used for the scientific, industrial and medical purposes.

2. Photoelectric absorption

If an incident X-ray photon has energy slightly greater than the binding energy of a bound atomic electron participating in the interaction, the photon transfers its energy to knock out the participating electron. The ejected electron is known as photoelectron. From the energy-momentum conservation law it may be noted that a free electron cannot absorb a photon. It means that, the electron should be bound within an atom for photon absorption. So, the probability of photoelectric effect is always higher for electrons located at lower electronic shells, which are closer to the atomic nucleus and hence are bound more strongly. The total energy of the ejected electron is

$$E_e = E_{inc} - E_B - T_N + m_o \qquad (1)$$

where E_{inc}, E_B, T_N and m_o are the incident photon energy, binding energy of electron, kinetic energy possessed by recoil nucleus and mass of electron, respectively. Therefore, the kinematic conditions for the minimum photon energy required for the photoelectric absorption to occur is

$$E_{inc} > E_B + T_N$$

In case the energy of the incident photon is not able to eject photoelectron, it may be partly absorbed by the atomic electron participating in the interaction and scattered out. The process is termed as Compton scattering. The scattering with no net absorption of photon by the atomic electrons termed as Rayleigh scattering. The cross sections for various photon-atom interaction processes in $_{59}$Pr, one of the elements of present concern, are plotted as function of energy in Fig. 1.

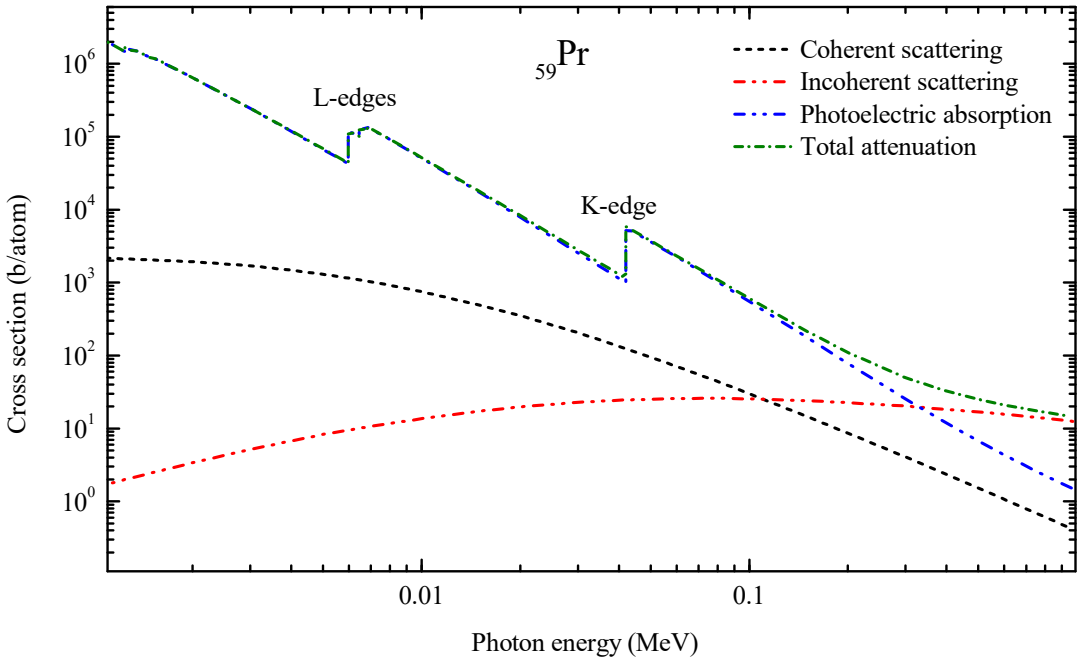

Fig. 1: The variation of cross section for various photon-atom interaction processes as a function of energy in case of $_{59}$Pr element.

During absroption Photoionization is prominent process if the energy of the incident photon matches with the ionizatinon threshold of the atoms in the material. The probability of the photoelectric effect is characterized by the cross section σ_{ph}, which rapidly increases with the atomic number Z. If the X-ray energy is much higher than the ionization potential Ij of a certain electronic shell j, the probability of X-ray absorption by electrons in this shell is $\sigma_{ph} \sim Z^5$ [**1**]. However, a quantitative comparison between different chemical elements is barely possible because of the great differences in the ionization potentials. Heavier elements such as, Pb absorb X-rays much more strongly than lighter elements. Photoelectric effect is a resonant process. The photoelectric cross section σ_{ph}, as a function of X-ray energy E_x, has sharp maxima at $E_x \approx I_j$ (Fig. 1). This forms the basis of selective used for X-ray filtering. The desired spectral lines from the polychromatic X-ray source can be obtained. Rayleigh scattering cross sections exceeds Compton scattering cross sections up to well above K-edge for all atomic numbers whereas the total cross section is photoelectric dominated. The total cross section curve attains a characteristic saw-tooth shape with the sharp discontinuity at the points where the incident energy matches with the ionization energy of electron in K, and L_i shells/subshells. At the first matching point the total cross section decreases suddenly because of the reason here the incident energy photons with low energy can no longer eject from K shell. Here photons continue to interact with more weakly attached electrons in lower energy L and M shells. These saw toothed discontinuities of the curve signifying the probability of photo electric absorption occurring energetically, are called as absorption edges. Therefore the photo electric absorption cross section falls off sharply as the photon energy decreases through this critical threshold value. The photoelectric absorption probability increases as the photon energy is decreased up to the limiting value of the absorption edge. Fewer electrons are available for absorption after crossing over the absorption edge and thus the probability of the process sharply decreased. In the high Z elements Rayleigh scattering provides a significant contribution just below the K shell ionization threshold. The Rayleigh scattering dominates Compton scattering till well above the K-shell ionization threshold afterwards the Compton scattering takes over. This is in general true for all elements. The total cross section is photo electric dominated up to photon energies increasing with atomic number, from 6 keV for $_2$He, to 25 keV for $_6$C and 700 keV for $_{92}$U. The Compton scattering becomes the domination process at ~100 keV for low Z elements and ~500 keV in case of high Z elements.

3. Scattering by atomic electrons

The incident photons generally scatter while interacting with the atomic electrons, In case the energy is less the photon interacts with the electron and emitted out with the same energy process is called elastic scattering. When interaction takes place with the atomic bound electrons it is referred to as Rayleigh scattering. In case some part of energy is consumed by the electron from incident photon, the process is termed as inelastic scattering. For atomic bound electrons, it is referred to as Compton

scattering. The theoretical approach to understand these processes is given in the following sections.

4. Rayleigh scattering

In Rayleigh scattering process, the incident photon imparts to the interacting electron some energy in the form of acceleration by the electromagnetic field associated with it. After interaction the photon emits photon having the same energy as the incident photon, means there is no net energy transfer from the photon to electron, resulting a phase relationship between the incident and scattered photons. Due to this coherence, the Rayleigh scattering process is called coherent scattering. Theoretically, two major approaches are developed to characterise the scattering: (i) Form-factor formalism, (ii) S-Matrix approach. These approaches are given as follows.

Form Factor formalism

J.J. Thomson gave a general formula for the scattering of unpolarised photons from the free electrons giving differential scattering cross section as

$$\frac{d\sigma_T}{d\Omega} = \frac{1}{2} r_o^2 \left(1 + \cos^2 \theta\right) \tag{2}$$

where, θ is the scattering angle through which the propagation direction of the incident photons changes and r_o is the classical radius of the free electron. For extended charge distributions, it is modified by including atomic form factor for a spherical charge distribution as given by

$$f(q) = 4\pi \int_0^\infty \rho(r) \frac{\sin(qr)}{qr} r^2 dr \tag{3}$$

where, $f(q)$ is the form factor, $\rho(r)$ is electron density at distance r from centre of the atom and q is momentum transferred to the atom during scattering. The $\rho(r)$ can be derived from the atomic ground state function given by

$$\rho(r) = \sum_{n=1}^{Z} |\psi_n(r)|^2 \tag{4}$$

For an atom containing Z electrons, the contributions of the individual electrons are added as,

$$4\pi \int_0^\infty \rho(r) r^2 dr = Z \tag{5}$$

The scattering cross section in the form factor formulation is obtained from the Thomson formula as

$$\left(\frac{d\sigma}{d\Omega}\right)_{el} = \left(\frac{d\sigma}{d\Omega}\right)_{T} \left|f(q)\right|^2 \tag{6}$$

The better results of the scattering cross section are found using form factor approximation for the incident photon having energy well above the *K*-shell threshold of the target atom. For small *q*, all the electrons contribute equally to the form factor but for large *q*, only the innermost electrons contribute. When the relativistic and non-relativistic individual electrons, and total atom wave functions are used to derive the charge density, the resulting form factors are termed as relativistic (RF) and non-relativistic (NF) form factors, respectively. These form factors are tabulated by Hubbell *et al*. [2,3]

Franz [4] considered the effect of electron binding energy and incorporated the correction for the same, the resulting form factor is called modified form factor (MF) given as

$$g(q) = 4\pi \int_0^\infty \rho(r) \frac{\sin(qr)}{qr} \frac{mc^2}{E_i - V(r)} r^2 dr \tag{7}$$

where, $\rho(r)$ is the charge distribution associated with the *i*th electron, $V(r)$ is the atomic potential and E_i is the binding energy of the *i*th electron. The contributions from the electrons of the individual subshells are calculated and added to deduce $g(q)$. The resulting differential scattering cross section for the unpolarized photons is given by

$$\left(\frac{d\sigma}{d\Omega}\right)_{MF} = \frac{d\sigma_T}{d\Omega} \left|g(q)\right|^2 \tag{8}$$

5. Compton scattering

Compton scattering is the process in which the participating electron absorbs a part of energy from the incident photon. The scattered photon has less energy than the incident one this is also called inelastic or incoherent scattering. In case, the excited electron jumps to a higher unoccupied energy level, the process is known as Raman scattering.

Scattering from free electrons

Compton scattering is a quantum electrodynamic interaction involving energy transfer between the interacting photon and electron. The process cannot be explained using classical electrodynamics theory but using quantum electrodynamics (QED) [19]. The incident photon interacts with a free electron and scattered with a loss of energy. The scattered photon energy (E_{sc}) is related to the incident energy (E_{in}) as

$$E_{sc} = \frac{E_{in}}{1+(1-\cos\theta)E_{in}/m_o c^2} \tag{9}$$

where, m_0c^2 is the rest mass energy of the electron (0.511 MeV) and θ is the scattering angle for the incident photon. The assumption for calculating the energy of the scattered photon is not precisely accurate because in reality the interaction of the incident photon takes place with moving bound electrons. The equation written for non-zero pre-collision energy and momentum of the electron is

$$p_z = -m_o c \frac{E_{in} - E_{sc} - E_{in}E_{sc}(1-\cos\theta)/m_o c^2}{\sqrt{E_{in}^2 + E_{sc}^2 - 2E_{in}E_{sc}\cos\theta}} \tag{10}$$

where p_z is simply referred as the projection of the electron momentum. It is interesting to notice that Eq. (10) reduces to (9) when $p_z = 0$. The electron momentum values are deduced from consistently symmetric distributions. These symmetric distributions are also known as Compton profiles that depend on the atomic subshell and target atom [20].

Klein and Nishina successfully applied Dirac's relativistic theory of electron for the scattering of photons by a free electron at rest to obtain a differential scattering cross section given as

$$\left(\frac{d\sigma}{d\Omega}\right)_{KN} = r_0^2\left(\frac{1}{1+\alpha(1-\cos\theta)}\right)^3\left(\frac{1+\cos^2\theta}{2}\right)\left\{1+\frac{\alpha^2(1-\cos\theta)^2}{(1+\cos^2\theta)(1+\alpha(1-\cos\theta))}\right\} \tag{11}$$

where $\alpha = E_{in}/m_0c^2$. The above equation is well known Klein-Nishina formula for the calculation of differential inelastic scattering cross section.

Scattering from bound electrons

The energy distribution profile of the Compton scattered photons is much broader than that of the incident photons. The momentum distribution of the bound electrons is a cause of this broadening [21]. The exact deviations of the inelastic scattering cross section due to electron binding energy effects are removed using the incoherent scattering function (ISF) approximation. The incoherent scattering of the incident photon from a bound electron modify the Klein-Nishina differential cross section

$$\left(\frac{d\sigma}{d\Omega}\right)_{inc} = \left(\frac{d\sigma}{d\Omega}\right)_{KN} S(q,Z) \tag{12}$$

where, $S(q,Z)$ is incoherent scattering function. The expression for the ISF in terms of atomic form factor can be expressed as

$$S(q,Z)=\sum_{m=1}^{Z}\sum_{n=1}^{Z}\left\langle \psi_{gs}\left|\exp\left[iq(r_m-r_n)/\hbar c\right]\right|\psi_{gs}\right\rangle-\left|f(q,Z)\right|^2 \tag{13}$$

where, the summations are over the number of electrons. The non-relativistic values of *S(q, Z)* has been tabulated by Hubbell *et al*. [2] for the values of q from .005 to 10^9 Å^{-1} for all elements with $1 \leq Z \leq 100$.

6. Scattering processes at near edge energies

When the energy of the incident photon is slightly less than the ionization threshold of the target atom, then participating electron takes energy and leaves the state vacant by going to the unoccupied energy levels. An electron from the upper shell fills the created hole, simultaneously. If the excited atom returns to the ground state via radiative transition then it is termed as resonant Raman scattering (RRS). If it comes to ground state via non-radiative transition, it is termed as the Auger resonant Raman effect [25].

Resonant Raman scattering

The resonant Raman scattering (RRS) is an inelastic scattering process and becomes significant as the incident photon energy is slightly less than the ionization threshold of the target atom [26]. The Raman scattering in the X-ray energy region are of two types, resonant Raman scattering (RRS) and resonant Raman Compton scattering (RRC). The resonant Raman scattering process results in a symmetric and sharp peak as the excited electron in a bound state whereas the resonant Raman Compton scattering results in asymmetric and broad peak as the excited electron is in a continuum state. The angular independence and frequency dependence of inelastic scattering explained with the X-ray scattering theory of anomalous dispersion is known as resonant Raman scattering. The RRS effect was observed for the first time by Sparks [27] and explained later by Bannet and Freund [28].

The Hamiltonian for the interaction of incident photon having potential vector $\boldsymbol{A}$ with electron having momentum $\boldsymbol{p}$ in the non-relativistic approximation is given as

$$H_{\text{int}}=-\frac{e}{mc}\boldsymbol{p.A}+\frac{e^2}{2mc^2}\boldsymbol{A.A} \tag{14}$$

The non-resonant scattering processes such as Rayleigh, Compton and normal Raman can be expressed in term of $\boldsymbol{A.A}$, in the first-order approximation [17] and the resonant inelastic scattering is expressed by the $\boldsymbol{p.A}$ term at the second-order expansion of the time-dependent perturbation theory. The double differential scattering cross section of resonant Raman scattering (RRS) can be given by Kramers-Hisenberg equation [29]

$$\frac{d^2\sigma_{RRS}}{dEd\Omega} = r_o^2\left(\frac{E}{E_o}\right)\frac{1}{m^2}\sum_i\left[\frac{\langle b|\boldsymbol{p}.\boldsymbol{e}_2|i\rangle\langle i|\boldsymbol{p}.\boldsymbol{e}_1|a\rangle}{E_a - E_i + E_o + i\Gamma_i/2}\right]^2 \quad (15)$$

where $\boldsymbol{e}_1$ and $\boldsymbol{e}_2$ are the unit polarization vectors for the incident photon with energy E_o and scattered photon with energy E respectively. The terms, E_a, E_i and E_b are the energies corresponding to the atomic states denoted as $|\ a >$ (initial state), $|\ i >$ (intermediate state) and $|\ b >$ (final state) respectively, Γ is the lifetime of the excited atomic state. In *KL*-RRS process, the virtual hole is created by the incident photon having energy just below the ionization threshold of the *K* shell and the created hole is subsequently filled either by an *L*-shell electron (*KL*-RRS) or an *M*-shell electron (*KM*-RRS) and so on. The *KL*-RRS process is shown schematically in Fig 1. Applying the dipole approximation and neglecting the weak non-resonant terms in Kramers-Hisenberg equation, the double differential scattering cross section for *KL*-RRS process can be written as

$$\left(\frac{d^2\sigma_{RRS}}{d\Omega dE}\right) = \frac{r_0^{\ 2}}{2}\frac{E}{E_0}\frac{(U_K + T_e)(U_K - U_L)}{(U_K - U_L - E)^2 + (\Gamma/2)^2}\, g_{1s,2p}\left(\frac{dg_K}{dT_e}\right)_{U_k + T_e} \quad (16)$$

where E is energy of the RRS scattered photon corresponding to the incident photon having energy E_o. According to the law of energy conservation, the average binding energy (U_L), the average kinetic energy of the ejected electron (T_e), the energy of Fermi level (E_F), E and E_o are related as E_o - U_L – $E_F = E + T_e$. The oscillator strength, $g_{1s,2p}$, is the oscillator

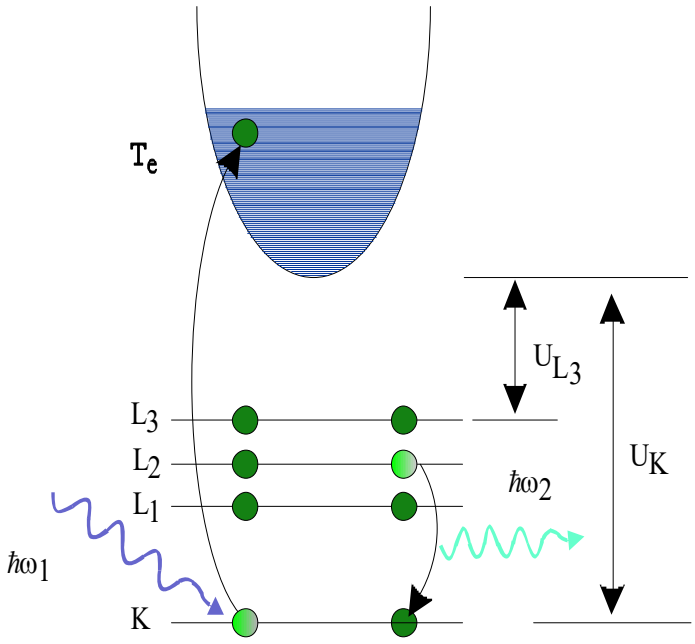

Fig. 2: Schematic representation of the KL_2 radiative RRS process.

strength between the $(1s)^{-1}$ and $(2p)^{-1}$ hole states and the oscillator density can be described as [30,31]

$$\left(\frac{dg_k}{dT_e}\right)_{u_K+T_e} = \frac{\tau_k(U_K+T_e)}{2\pi^2\hbar c r_0} \tag{17}$$

$$g_{1s,2p} = \frac{1}{2}\frac{\hbar c\,\Gamma_{K\alpha}}{r_0(U_K-U_L)^2} \tag{18}$$

where $\Gamma_K, \tau_K(U_K+T_e)$ and $\Gamma_{K\alpha}$ are the total K-shell width, the photoionization cross section of the K shell at the energy U_K+T_e and width of the $K\alpha$ fluorescence line respectively. As the oscillator density depends upon the density of empty states in the continuum, so it may be assumed constant if the contribution of the final state is ignored and thus an average kinetic energy (T_e) for the ejected electron may be considered. From Eq. (18) and assuming a constant oscillator density, the double differential cross section can be written as

$$\left(\frac{d^2\sigma_{RRS}}{d\Omega dE}\right) = \Gamma_{K\alpha}\frac{\tau_K(U_K+T_e)}{8\pi^2(U_K-U_L)}\frac{E}{E_0}\frac{U_K-U_L+E_0-E}{(U_K-U_L-E)^2+(\Gamma/2)^2} \tag{19}$$

It is clear from Eq. (19), the RRS emission spectrum exhibits Lorentzian distribution which is centered at U_K - U_L. However, the energy conservation imposes a limit on the RRS peak profile distribution and the maximum value of RRS peak is called cutoff energy $E_s^{\max}$ given by following expression

$$E_s^{\max} = E_0 - U_L \tag{20}$$

Due to this cutoff energy value, the RRS peak shows a left-wing of the Lorentzian distribution. The total RRS cross section per unit sold angle is obtained on integrating the Eq. (19) for all possible photon energies of the scattered radiation given as

$$\frac{d\sigma_{RRS}}{d\Omega} = \int_0^{E_s^{\max}} \frac{d^2\sigma_{RRS}}{d\Omega dE_s} dE_s \sim \frac{1}{U_K - E_o} \tag{20}$$

Recent review of the theoretical approach infers that RRS exhibits an isotropic emission independent from the incident photon polarization state. Aberg and Tulkki [32-34] have predicted that polarized radiations should exhibit an anisotropic RRS emission due to the interference between the non-

resonant and the resonant terms of the KH formula and is not incorporated in the earlier approach. The modified form of the RRS differential cross section can be rewritten as

$$\left(\frac{d^2\sigma_{RRS}}{d\Omega dE_s}\right)_{pol} = \frac{d^2\sigma_{RRS}}{d\Omega dE_s}\left[B(f-1)+(1+B)^2\right] \tag{21}$$

where B denotes the influence of the non-resonant terms of the KH formula and can be obtained as

$$B=\frac{U_K-U_L-E_s}{U_K-U_L+E} \tag{22}$$

The angular dependence effect on the RRS in conjunction with polarization influence is introduced by the parameter f and the formula is further modified according to the orientation of the scattering plane with respect to the polarization plane of the incident photon beam as follows [35]

$$f_{\parallel(\perp)} = \cos^2\theta\,(\mp)\,P\sin^2\theta \tag{23}$$

where symbols, || and ⊥ indicate the parallel and perpendicular orientation of the scattering plane, P is the effective linear polarization for the incident beam. It is well known that the unpolarized beam can be expressed as a superposition of two perpendicular polarized constituents, *i.e.*, $I_{unpol}=\frac{1}{2}I_{\parallel}+\frac{1}{2}I_{\perp}$. Therefore, the RRS cross section in differential form for the unpolarized incident beam can be written as

$$\left(\frac{d^2\sigma_{RRS}}{d\Omega dE_s}\right)_{pol} = \frac{d^2\sigma_{RRS}}{d\Omega dE_s}\left[1+B(1+B)\right] \tag{24}$$

Just above the absorption edge ($E_x \geq I_j$), there are small systematic oscillations in absorption cross section (Fig 2), which are called extended X-ray absorption fine structure (EXAFS). This phenomenon is related to the interference between the secondary electrons ejected at the first stage of the photoelectric effect. Some of these electrons experience scattering by neighbor atoms. EXAFS originates in the interference between the scattered and nonscattered electrons. Therefore, EXAFS oscillations in the cross section σ_{ph} are sensitive to the distances between neighboring atoms, *i.e.*, to short-range atomic order. EXAFS has become a leading method for studying the short-range atomic structure in different materials (crystalline, amorphous, and liquids [35]).

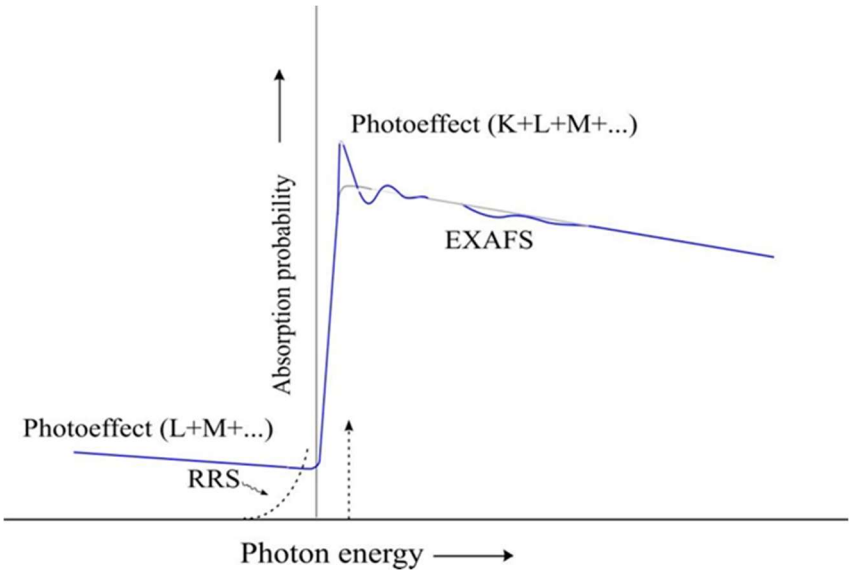

Fig. 3: The contribution of various processes to the absorption in the vicinity of the *K* shell ionization threshold of an element. EXAFS region involving oscillations in X-ray absorption is marked by a dashed arrow on the right-hand side of the absorption edge.

7. Scattering from an aggregate of atoms

Material is meant to be an aggregate of atoms, which may be crystalline or amorphous in nature. When scattering occurs from a solid or liquid consisting of an aggregation of atoms, other scattering effects may be noted. In case of crystalline materials, the atoms have periodically spaced structure called lattice. When the wavefront of X-rays impinges on this set of atoms, each atom scatters X-rays. If the atoms are centred on points in a plane, for example, a plane in a lattice array corresponding to a crystallographic plane (*hkl*), two directions of scattering have special properties, as shown in Fig. 3. In both these directions, the distance from the original wave front, to an atom, and on to a new wave front is the same for all atom locations in the plane. These directions correspond, respectively, to a continuation of the beam in the original direction, and to a reflection of the beam by the plane on which the atoms lie. The scattering by atoms in a plane is, therefore, equivalent to reflection by the plane. A lattice array of atoms have equally spaced parallel planes. The waves associated with photons scattering from each of the regularly spaced atoms in crystal show coherence and result in the constructive interference (diffraction) in few directions. This results in the sharp peak maxima in the pattern, giving the characteristics of the structure for the material according to Bragg's Diffraction law given by

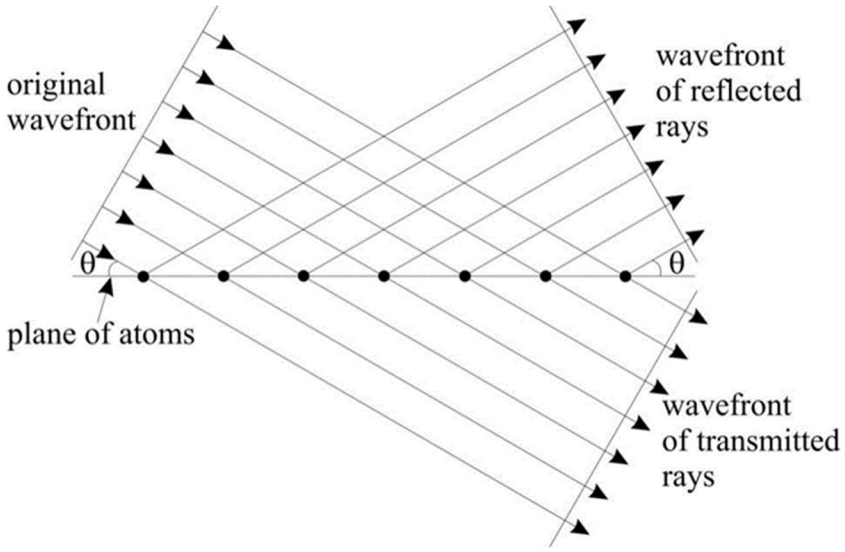

Fig. 4: Two directions of wavefronts after interacting with a plane of atoms.

$$2d\sin\theta = n\lambda \quad (25)$$

where, d is the spacing between diffracting planes, θ is the incident angle, n is the integer characterising the order of the diffraction, λ is the wavelength of the incident beam. This

process is called Bragg's diffraction. The coherent/incoherent intensity ratio will vary widely with scattering angle and will also depend upon the crystallinity and average atomic number of the specimen, as well as the energy of the scattering radiation. In specimens of finite thickness, absorption of the incident and scattered radiation in the specimen must also be considered. The X-ray diffraction effect is used in the wavelength-dispersive spectrometer as a basis for spectral separation. A single crystal is cleaved such that a selected set of atomic planes (*hkl*) of interplanar spacing parallel with the surface. This crystal is used to diffract the polychromatic beam of fluorescence emission from the specimen, and rotating the crystal to an appropriate angle θ will cause a given wavelength λ to be diffracted at angle 2θ, provided that the Bragg relation (eq. 25) is satisfied.

X-ray diffraction in polycrystalline materials

It is clear that the X-ray diffraction results from an electromagnetic wave (the X-ray) impinging on a regular array of scatterers (the repeating arrangement of atoms within the crystal). For polycrystalline materials, analytic solutions for diffraction intensity can be obtained in two extreme cases: ideal mosaic crystals, and random distribution of small crystallites which produces the so-called powder diffraction pattern. While explaining the models in case of macroscopic samples, X-ray absorption within a material should be taken into account due to larger thickness of polycrystalline sample than the X-ray absorption length in the material. [37]

(a) Ideal Mosaic crystal

Consider small crystallites, each having volume V, that are slightly misoriented with respect to each other (Fig.4). The characteristic misorientation angle Ω_m defines the so-called crystal mosaicity. The geometry permits individual crystallites to scatter independently. The angle the angle Ω_m is less than the divergence $\Delta\alpha$ of the incident beam, so that all crystallites diffract simultaneously. So, in this model, the contributions of all small crystallites within the sample of thickness T are added, taking into account the exponential attenuation of the incident and diffracted beams with depth z due to X-ray absorption.

If the incident beam has the cross-sectional area S_0 (Fig.5) then the number dN of crystallites within infinitesimally thin layer dz which scatters X-rays by the angle 2Θ is

$$dN = \frac{S_0}{V \sin\Theta} dz \tag{26}$$

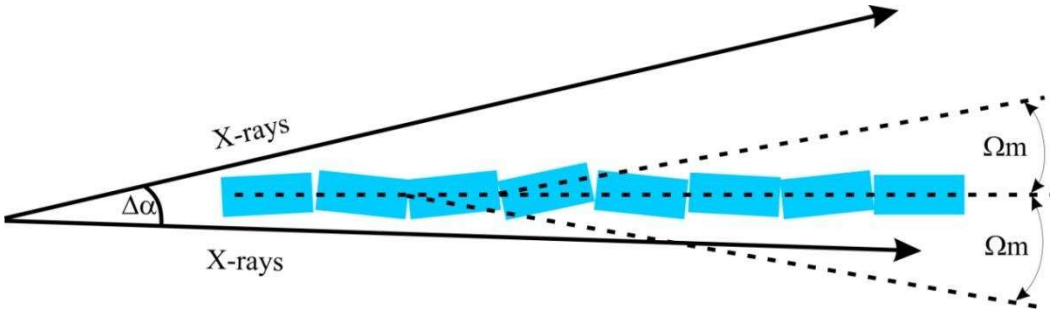

Fig.5: Ideal mosaic crystal

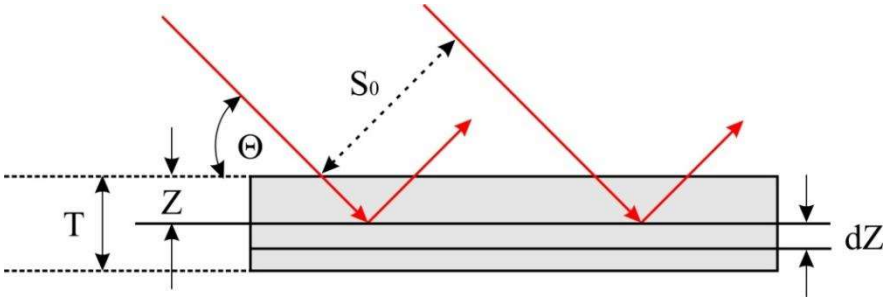

Fig.6: Symmetric Bragg scattering geometry

If this layer is located at depth z, then its contribution dI to diffraction intensity is

$$dI = E_{SC} \exp\left(-\frac{2\mu z}{\sin\theta}\right) dN \tag{27}$$

where E_{sc} is the scattering power of a small crystal and is given by the equation

$$E_{SC} = \frac{|F|^2 r_0^2 \lambda^3 V}{\sin(2\Theta_B) V^2} \left(\frac{1+\cos^2 2\theta_B}{2}\right) \exp(-2W) I_0 \tag{28}$$

Substituting the value of dN and E_{sc} and integrating over sample thickness T, the diffraction power E_{mc} for an ideal mosaic crystal $2\Theta \approx 2\Theta_B$ is given by

$$E_{mc} = \int_0^T E_{SC} \exp\left(\frac{-2\mu z}{\sin\theta_B}\right) dN = \frac{|F|^2 r_0^2 \lambda^3}{\sin(2\Theta_B) V^2} P_p \left(\frac{1-\exp(-2\mu t/\sin\theta_B)}{2\mu}\right) \exp(-2W) S_0 I_0 \tag{29}$$

where P_p is the polarization factor for a non-polarized incident beam.

$$P_p = \frac{1}{2}\left[1+\cos^2(2\Theta_B)\right] \tag{30}$$

The diffraction does not depend on the sample thickness T; its role is played by the parameter $1/2\mu$.

(b) Powder Diffraction

For powder diffraction, three additional issues have to take into account:

i) Random distribution of crystallite orientation within a sample;

ii) X-ray scattering within a diffraction cone;

iii) Multiplicity factor.

Item (i) means that only those crystallites will participate in the diffraction process in which the chosen (*hkl*) planes meet incident X-rays at the correct entrance angle θ_B. In order to take account of this point, let us designate the angle between the normal to parallel planes (*hkl*) and the wave vector of the incident X-rays as Ψ (Fig.6 (a)). The probability to find this normal at an angle between Ψ and Ψ+dΨ is defined by the element of solid angle $d\Omega$, given by

$$d\Omega = 2\pi \sin\Psi d\Psi = 2\pi \sin(90^\circ - \theta_B) d\Psi = 2\pi \cos\theta_B d\Psi \tag{31}$$

Item (ii) is related to the fact that the diffraction pattern from a random powder has axial symmetry with respect to the wave vector $\mathbf{k}_i$ of the incident X-ray beam. This means that the diffraction intensity from a certain crystallographic plane (*hkl*) is distributed along a conical surface (Fig.6 (b)). The cone tip is at the center of the sample. In plane projection, the diffraction intensity forms the so-called Debye-Scherrer rings. This distribution should be taken into account in diffraction measurements

utilizing point detector scans, since in the latter only a small part ζ of the diffraction intensity is entering detector after passing through the receiving slit S_d in front of it

$$\zeta = \frac{S_d}{2\pi R_d \sin 2\theta_B} \tag{32}$$

where R_d is the length of the detector arm.

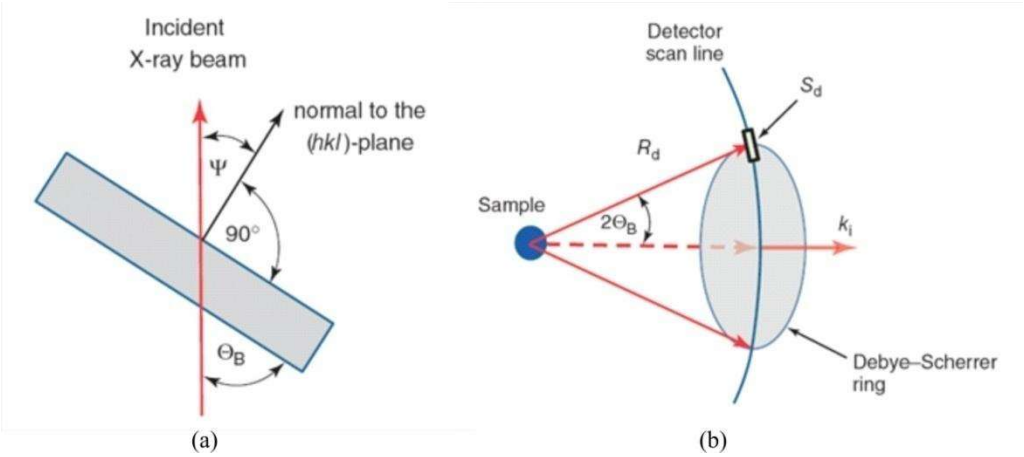

Fig.7: Illustration for (a) Random distribution of crystallite orientation within a sample (b) X-ray scattering within a diffraction cone. Wave vector of the incident X-ray beam in denoted as $\mathbf{k}_i$.

Item (iii) reflects the fact that powder diffraction deals with Debye–Scherrer rings whose radii are defined by crystal *d*-spacings. If different combinations of Miller indices (*hkl*) produce identical *d*-spacings, these planes will contribute to the same Debye–Scherrer ring, thus increasing its intensity. To take this effect into account, the multiplicity factor P_m is equal to the number of equivalent planes that are produced from the initial plane by all symmetry operations included in the crystal point group. The multiplicity factor differs for different types of crystallographic planes and depends also on the symmetry system to which investigated crystal belongs. Considering all the above factors, the powder diffraction intensity E_p is expressed as

$$E_p = K_e \frac{|F|^2 r_o^2 \lambda^3}{(V_c)^2 \sin\theta_B \sin 2\theta_B} P_m \exp(-2W)\left(\frac{1-\exp(-2\mu t/\sin\theta_B)}{2\mu}\right)\left(\frac{1+\cos^2 2\Theta_B}{2}\right) \quad (33)$$

Where the coefficient K_e unifies a number of experimental parameters, such as incident X-ray intensity (I_o), cross-sectional area (S_o) of the beam irradiating whole crystal R_d, and S_d, which are not varied in a particular measurement.

Kinematic diffraction theory is provided with diffraction peak positions (via Bragg law) and diffraction intensity. Three main parameters describing each diffraction line are intensity (peak or integrated) I, peak width Γ, and angular peak position Θ. The latter, $\Theta=\Theta_B+\delta\Theta$, is composed of the expected Bragg position Θ_B and its deviation $\delta\Theta$. Measurement of all these parameters is the basis of important applications of X-ray diffraction to materials science. Specifically, the peak intensities I and the peak positions Θ_B are used for structure determination and phase analysis of polycrystalline samples. Deviations of peak intensities from those predicted by powder diffraction theory are treated within texture analysis. The widths Γ of the diffraction profiles are used for line-broadening analysis aimed at extracting crystallite size and averaged microstrain fluctuations. The angular deviations $\delta\Theta$ are the basis of the residual strain/stress analysis.

8. Photon absorption

For a material comprising only one type of atoms with atomic concentration considering as c_a per unit volume. X-rays with intensity I (per unit area) entering the material normal to the entrance surface (Fig. 8) will be attenuated by an amount dI when passing through a material layer with thickness dz. For an infinitesimally thin layer, the attenuations caused by the individual atoms can be summed

$$dI = -I\sigma_{ph} c_a dz \quad (34)$$

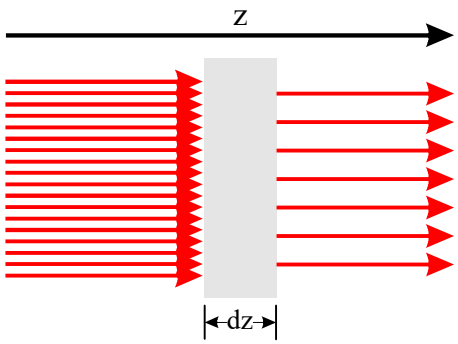

Fig. 8: X-ray attenuation when passing through material at normal incidence.

The negative sign in eq. (34) reflects the decrease in the beam intensity after passing through the

layer *dz*. Integrating eq. (34) yields the exponential attenuation of X-ray intensity with depth *z* as

$$I = I_0 \exp\left(-\sigma_{ph} c_a z\right) = I_0 \exp\left(-\mu z\right) \quad (35)$$

where I_0 is the incident X-ray intensity at z=0. The product of the cross section σ_{ph} and atomic concentration c_a

$$\mu = \sigma_{ph} c_a \quad (36)$$

has the dimension of inverse length and is called the linear absorption coefficient μ(cm^{-1}). The parameter $1/\mu$ defines the characteristic thickness of a material layer that causes attenuation of X-ray intensity e (=2.718) times that at normal incidence. For example, in Si, $1/\mu \approx 70$ μm for Cu-$K\alpha$ radiation (λ=1.54 Å), while $1/\mu \approx$ 700 μm for Mo-$K\alpha$ radiation (λ=0.71 Å). The absorption in a material is also taken as a measure of mass attenuation coefficient defined as $\mu_m = \mu/\rho$, with units (cm^2/g). In these units, the value of mass attenuation coefficient, μ_m is independent of the physical state of the absorber. The value of the μ_m in case of multielemental absorber can be written in terms of the values of μ_m for the constituent elements, *viz*., $\mu_{compd} = \sum \mu_i w_i / \sum w_i$, where w_i is the weight of *i*th element in the target.

Absorption in Bragg scattering geometry

For analysis of the diffraction intensity, another characteristic depth Λ_a is introduced, which also causes 2.718 (e) times attenuation of X-ray intensity but takes into account actual trajectories of the incoming and diffracted X-rays in the symmetric Bragg scattering geometry (Fig. 9)

$$\Lambda_a = \frac{\sin\Theta}{2\mu} \quad (37)$$

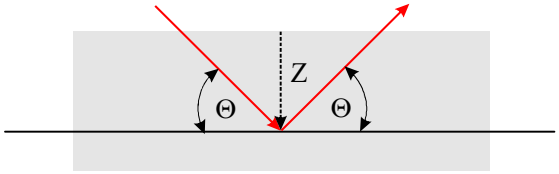

Fig. 9: X-ray penetration depth in a symmetric Bragg scattering geometry

where Θ is the diffraction angle defined at a fixed wavelength λ by the *d*-spacing. So, in this geometry, the exponential attenuation of the diffraction intensity I_d with depth *z* due to absorption is expressed as

$$I_d = I_{d0} \exp\left(-\frac{z}{\Lambda_a}\right) \quad (38)$$

In asymmetric Bragg scattering geometry, that is, when the atomic planes used for X-ray diffraction meet the surface of the sample at some angle $\alpha \neq 0$ (Fig.10), the characteristic absorption depth Λ_a is

$$\Lambda_a = \left\{\mu\left(\frac{1}{\sin(\theta-\alpha)}\right)+\left(\frac{1}{\sin(\theta+\alpha)}\right)\right\}^{-1} \quad (39)$$

If the glancing angle, $\omega = \theta - \alpha$, is very small (about 1° or less), the penetration depth, Λ_a, is considerably reduced down to the sub micrometer level

$$\Lambda_a \approx \frac{\omega}{\mu} \quad (40)$$

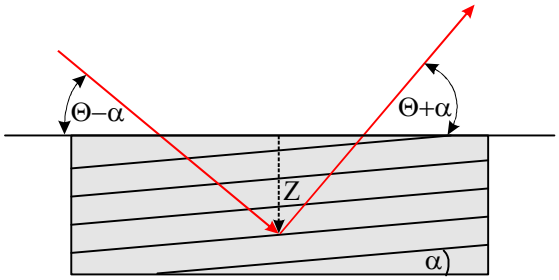

Fig. 10: X-ray penetration depth in an asymmetric Bragg scattering geometry.

and hence the sensitivity of X-ray diffraction to thin layers of materials may be significantly enhanced. This is the basis of the glancing-incidence diffraction method for studying thin polycrystalline films. The glancing-incidence condition for single crystals, $\omega = \Theta - \alpha \approx 0$, that is,

$$\alpha = \Theta = \Theta_B = \sin^{-1}\left(\frac{\lambda}{2d}\right) \quad (41)$$

can easily be achieved when working at synchrotron beam lines by changing the X-ray wavelength λ.

9. Conclusions

It is concluded that the photon-atom interaction processes are discussed, in which, particular stress is given on the interactions involving scattering of photon. The scattering of photons is really

important to understand the concepts of X-ray spectrometry and crystallography, whether these are related to scattering by electrons, atoms or a complete crystals. Theoretical aspects are studied and discussed. Generally, the results from experimental measurements are compared to the theoretically calculated parameters to check the accuracy and conflicts arising from the comparisons lead to new problems for researchers.

References

1. V. B. Berestetskii, E. M. Lifshitz, and L. P. Pitaevskii, Quantum Electrodynamics, Pergamon Press, Oxford (1982).
2. J. H. Hubbell, W. J. Veigele, E. A. Briggs, R. T. Brown, D. T. Cromer and R. J. Howerton, J. Phys. Chem. Ref. Data 4 (1975) 471, 6 (1977) 615(E).
3. J. H. Hubbell and I. O. Verbro, J. Phys. Chem. Ref. Data 8 (1979) 69.
4. W. Franz, Z. Phys. 98, (1936) 314.
5. D. Schaupp, M. Schumacher, F. Smend, P. Rullhusen and J. H. Hubbell, J. Phys. Chem. Ref. Data 12 (1983) 467.
6. D. T. Cromer and D. A. Liberman, J. Phys. Chem. Ref. Data 54 (1970) 1891.
7. D. T. Cromer and D. A. Liberman, Acta Cryst. A 37 (1981) 267.
8. D. T. Cromer, J. Appl. Cryst. 16 (1983) 437.
9. B. L. Henke and D. T. Atwood, Am. Ins. Phys. Conf. Proc. No. 75 (1981) 340.
10. B. L. Henke, P. Lee, T. J. Tanaka and B. K. Fujikawa, At. Nucl. Data Tables 27 (1993) 1.
11. B. L. Henke, E. M. Gullikson and J. C. Davis, At. Nucl. Data Tables 54 (1993) 181.
12. L. Kissel, B. Zhou, S. C. Roy, S. K. Sen Gupta and R. H. Pratt, Acta Cryst. A 51 (1995) 271.
13. L. Kissel and R. H. Pratt, Acta Cryst. A 46 (1990) 170.
14. M. Deutsch and M. Ahrt, Phys. Rev. B 37 (1988) 2701.
15. L. Gerward, G.Thuesen, M. S. Jensen and L. Astrup, Acta Cryst. A 35 (179) 852.
16. D. C. Creagh, Phys. Lett. A 103 (1984) 52.
17. P. P. Kane, L. Kissel, R. H. Pratt and S. C. Roy, Phys. Rep. 140 (1986) 75.
18. L. Kissel, Lawrence Livermore National Laboratory, USA (1997), Private communication, website: http://www-phys.llnl.gov/Research/scattering/.
19. B. J. McParland, Nuclear Medicine Radiation Dosimetry: Advance Theoretical Principle, Springer.
20. B. Williams, ed., "Compton Scattering: The Investigation of Electron Momentum Distributions," McGraw-Hill (New York), 1977.
21. J. W. M. Dumond, Phys. Rev. 5 (1933) 1.
22. I. B. Whittingham, J. Phys. A 4 (1971) 21.
23. I. B. Whittingham, Aust. J. Phys. 34 (1981) 163.
24. T. Suric, P. M. Bergstrom, K. Pisk and R. H. Pratt, Phys. Rev. Lett. 67 (1991) 189.
25. G. S. Brown, M. H. Chen, B. Crasemann and G. E. Ice, Phys. Rev. Lett. 45 (1980) 1937.

26. A. Kotani and M. Shin, Rev. Mod. Phys. 73 (2001) 203.
27. C. J. Sparks and G. E. Ice, Ind. J. Phys. 71B (1997) 393.
28. Y. B. Bannett and I. Freund, Phys. Rev. Lett. 34 (1975) 372.
29. H. A. Kramers and W. Heisenberg, Z. Phys. 31 (1925) 681.
30. A. G. Karydas, S. Galanopoulos, Ch. Zarkadas, T. Paradellis and N. Kallithrakas-Kontos, J. Phys. Cond. Matt. 14 (2002) 12367.
31. P. Suortti, Phys. Status Solidi 91 (1979) 657.
32. J. Tulkki and T. Aberg, J. Phys. B 13 (1980) 3341.
33. J. Tulkki, J. Phys. B 17 (1984) 3493.
34. T. Aberg and J. Tulkki, in Atomic Inner-shell Physics, edited by B. Crasemann (Plenum, New York, 1985), Chap. 10.
35. H. Czerwinski, F. Smend, D. Schaupp, M. Schumacher, A.H. Millhouse and H. Schenk-Strauss, Z. Phys. A 322, 183 (1985).
36. G. Bunker, Introduction to XAFS: A Practical Guide to X-ray Absorption Fine Structure, Cambridge University Press, Cambridge (2010).
37. E. Zolotoyabko, Basic concepts of X-ray diffraction, Wiley-Germany (2014).
38. P. A. M. Dirac, Principle of Quantum Mechanics, 3rd ed., Oxford, 1947.
39. E. J. McGuire, Phys. Rev. A 3 (1971) 587.
40. E. J. McGuire, Phys. Rev. A 179 (1972) 1043.
41. S. Puri, D. Mehta, B. Chand, N. Singh and P.N. Trehan, X-ray Spectrom. 22 (1993) 358.
42. J. L. Campbell, At. Data Nucl. Data Tables 85 (2003) 291.
43. J. H. Scofield, At. Data Nucl. Data Tables 14 (1974) 121.
44. J. H. Scofield, Phys. Rev. A 10 (1974b) 1507; erratum, Phys. Rev. A 12 (1975) 345.
45. J. L. Campbell and J.X.Wang, At. Data Nucl. Data Tables 43 (1989) 281.
46. J. H. Scofield, Lawrence Livermore laboratory, Report no. 51236 (1973) unpublished.
47. S. Puri, B. Chand, D. Mehta, M.L. Garg, N. Singh and P.N. Trehan, At. Data Nucl. Data Tables 61 (1995) 289.
48. J. H. Scofield, Phys. Rev. A 9 (1974) 1041.
49. J. H. Hubbell, P. N. Trehan, N. Singh, B. Chand, D. Mehta, M. L. Garg, R.R. Garg, S. Singh and S. Puri, J. Phys. Chem. Ref. Data 23 (1994) 339.